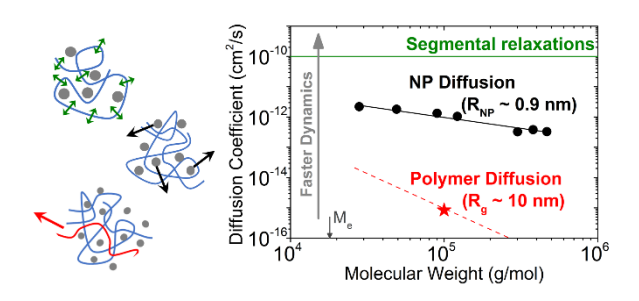
Multiscale Dynamics of Small, Attractive Nanoparticles and Entangled Polymers in Polymer Nanocomposites

Eric J. Bailey[‡], Philip J. Griffin[‡], Russell J. Composto, and Karen I. Winey*

Department of Materials Science and Engineering, University of Pennsylvania, Philadelphia, Pennsylvania 19104, United States

^{*}Author to whom correspondence should be addressed. Electronic address: winey@seas.upenn.edu



For Table of Content use only

Abstract:

Polymer segmental dynamics, center-of-mass chain diffusion, and nanoparticle (NP) diffusion are directly measured in a series of polymer nanocomposites (PNC) comprised of very small (radius ≈ 0.9 nm) octaaminophenyl silsesquioxane (OAPS) NPs and poly(2-vinylpyridine) (P2VP) of varying molecular weight. With increasing OAPS concentration, both the segment reorientational relaxation rate (measured by dielectric spectroscopy) and polymer chain center-of-mass diffusion coefficient (measured by elastic recoil detection) are substantially reduced, with reductions relative to bulk reaching ~80% and ~60%, respectively, at 25 vol% OAPS. This commensurate slowing of both the segmental relaxation and chain diffusion process is fundamentally different than the case of PNCs composed of larger, immobile nanoparticles, where the motion of most segments remains relatively unaltered even though chain diffusion is significantly reduced. Next, using Rutherford backscattering spectrometry to probe the NP diffusion process, we find that small OAPS NPs diffuse anomalously fast in these P2VP-based PNCs, reaching diffusivities 10-10,000 times faster than predicted by the Stokes-Einstein relation assuming the melt zeroshear viscosity. The OAPS diffusion coefficients are found to scale very weakly with molecular weight, M_w-0.7±0.1, and our analysis shows that this characteristic OAPS diffusion rate occurs on intermediate microscopic timescales, lying between the Rouse time of a Kuhn monomer τ_0 and the Rouse time of an entanglement strand τ_e . Our findings suggest that transport of these very small, attractive nanoparticles through well-entangled polymer melts is consistent with the recently reported vehicle mechanism of nanoparticle diffusion.

Introduction:

Understanding nanoparticle (NP) and polymer dynamics over their hierarchy of length and time scales is a complex problem relevant to drug delivery, filtration technology, and the properties and processability of polymer nanocomposites (PNCs). $^{1-5}$ Because NPs and polymers share overlapping energy, length, and time scales, their motional processes are interrelated and therefore significantly impact each other. This is especially true for very small NPs in well-entangled polymer matrices, where the radius of the nanoparticle (R_{NP}) is on the order of the radius of gyration of the polymer (R_{g}) or the entanglement tube diameter (d_{tube}).

It is now well established that polymer dynamics at small length scales (e.g. segmental relaxations) are perturbed near a NP surface^{3,4,6–8} and are highly dependent on system-specific parameters, including NP-polymer interfacial interaction^{9,10} and NP size^{11,12}. For example, poly(2-vinylpyridine) (P2VP) segmental dynamics are ~100 times slower near the surface of moderately-sized, attractive silica NPs (SiO₂, $R_{NP} = 13$ nm), but remain bulk-like beyond ~5 nm from the NP surface.¹³ Similar behavior is reported in MD simulations of attractive PNCs.¹⁴ However, the magnitude of reduced segmental dynamics is dependent on the NP-polymer interaction while the length-scale over which relaxations are perturbed is nominally independent of interactions and reported as ~3 nm.¹⁴ For attractive PNCs with NPs on the order of the segment size ($R_{NP} = 0.9$ nm), experiments coupled with theory and simulations designed to mimic the sizes and interactions in the experimental system report categorically different behavior as compared to PNCs with larger NPs.¹² For example, in PNCs with smaller NPs, segmental relaxations slow precipitously and become more dependent on temperature (more fragile) with increasing NP concentration (ϕ_{NP}).¹² In addition, the glass transition temperature increases up to 30°C at $\phi_{NP} = 54$ vol% but the step in specific heat capacity remains unchanged, both of which are not true for PNCs with larger NPs.¹²

At longer length scales, polymer chain diffusion through PNCs has been measured as a function of NP concentration¹⁵, NP and polymer size¹⁶, NP-polymer attraction¹⁷, and NP interface softness¹⁸. In each case, the polymer chain diffusion coefficient through PNCs decreases with decreasing interparticle

separation distance (achieved by increasing ϕ_{NP} or decreasing R_{NP}). It is important to note that the NPs in these experiments are effectively immobile on the timescale of polymer diffusion, with the exception of a recent subset of systems with anisotropic NPs.¹⁹

It is crucial to consider the hierarchy of polymer dynamics from the segment to chain scale when studying the diffusion of NPs in a polymer melt because the relevant polymer dynamics depend on the size of the NP, polymer chain length, and NP-polymer interaction. $^{20-24}$ A continuum hydrodynamic description of the translational diffusion of spherical particles, D_{SE} , in a polymer melt is given by the Stokes-Einstein (SE) equation with static boundary conditions:

$$D_{SE} = \frac{k_B T}{6\pi \eta_0 R_{NP}} \tag{1}$$

where k_BT is the thermal energy term and η_0 is the zero-shear viscosity of the polymer medium.²⁵ However, the SE prediction often fails to describe NP diffusion in polymer melts, especially when $R_{\rm NP} < R_{\rm g}$ (or $d_{\rm tube}$) or in systems with strong NP-polymer attraction.^{21,26,27} Both of these cases, small NPs and strong interactions, are especially important to understand because it is at these limits where uniform NP dispersion is most often realized.^{3,28} It has been shown that athermal gold NPs ($R_{NP} = 2.5 - 10$ nm) diffuse in entangled poly(butyl methacrylate) melts ($M/M_e = 12$, where M_e is the entanglement molecular weight) approximately 10 – 100 times faster than the SE prediction.²⁹ Diffusion of small NPs in athermal or repulsive polymer melts at timescales faster than D_{SE} was also observed in MD simulations^{30,31} and predicted in self-consistent generalized Langevin equation theory. ²¹ To describe the diffusion of small NPs, η_0 is sometimes replaced with a length-scale-dependent viscosity smaller than the macroscopic value and corresponding to approximately the NP size, however, Equation 1 is commonly used for comparison. ^{21,23,24,30} A more recent theory by Yamamoto et al. that includes NP-polymer attraction predicts two competing mechanisms of NP motion called core-shell and vehicle diffusion.²⁶ In the core-shell mechanism, NPs and adsorbed polymer chains diffuse together with an effective size larger than R_{NP}. This core-shell diffusion has been observed experimentally in mixtures of P2VP and SiO₂ (R_{NP} > R_g), where SE behavior was retained by using an increased effective NP size to capture the presence of an irreversibly

bound polymer layer.³² In vehicle diffusion, NPs are predicted to diffuse with the local polymer environment until the NP desorbs and re-adsorbs in a new environment, which usually leads to fast NP diffusion relative to Equation 1.²⁶ A crossover between core-shell (where $D/D_{SE} \sim 0.6$) and vehicle diffusion (where $D/D_{SE} \sim 20$) was recently measured using dynamic light scattering (DLS) in mixtures of sticky NPs ($R_{NP} = 0.9$ nm) in polypropylene glycol (PPG) melts with $M/M_e < 6.^{33}$

In this article, we combine measurements of polymer dynamics at the segment and chain scale with measurements of NP diffusion to probe polymer and NP dynamics in PNCs with small nanoparticles (R_{NP} << R_g), entangled polymers, and attractive NP-polymer interactions. The PNCs are comprised of well-entangled poly(2-vinylpyridine) (P2VP) (M/M_e \approx 1 – 26 where M_e = 18 kg/mol and R_g = 4.5 – 18.7 nm)³² and octaaminophenyl silsesquioxane (OAPS) NPs ($R_{NP} \approx 0.9 \text{ nm}$)¹². The polymer dynamics on the chain-scale are suppressed by up to ~60% relative to bulk at NP concentrations of 25 vol%. This reduction in chain dynamics is largely due to a slowing of polymer segmental dynamics, which likely results from favorable pyridine-amine interactions. In addition, relative to the hydrodynamic SE prediction based on the NP size and zero-shear melt viscosities, the NP diffusivity is dramatically enhanced (up to a factor of 10,000). NP diffusion coefficients in this system are modestly dependent on polymer molecular weight, scaling as $\sim M_w^{-0.7\pm0.1}$, which is comparable to recent theoretical predictions of the vehicle mechanism in well-entangled attractive polymer melts. ²⁶ By measuring and correlating multi-scale polymer and NP dynamics, we conclude that the transport of small, attractive NPs in entangled polymer melts occurs via the vehicle mechanism, where NPs diffuse via successive adsorption/desorption events that likely take place on Rouse time scales.

Experimental Section:

Materials and PNC preparation: All poly(2-vinylpyridine) (P2VP) was received from Polymer Source or Scientific Polymer Products and used as received. All polymer molar mass moments and distributions were verified by gel permeation chromatography (relative to narrow polystyrene standards), and all dispersities were < 1.3, as listed in Table S1. Partially deuterated poly(2-vinylpyridine) (dP2VP) was synthesized at the Center for Nanophase Materials Science at Oak Ridge National Laboratory. The deuterium to hydrogen ratio (measured by elastic recoil detection) is approximately 1:2 and the weight-averaged molecular weight and dispersity (measured by GPC) are 100 kg/mol and 1.2, respectively. Dry octaaminophenyl silsesquioxane (OAPS) powder was used as received.

PNCs were fabricated by solution mixing and drying. Solutions of OAPS in MeOH ($c_{OAPS}\sim20$ g/L) and P2VP in MeOH ($c_{P2VP}\sim50$ g/L) were fabricated and allowed to stir for several hours. Once completely dissolved, the requisite amount of OAPS/MeOH was added dropwise to P2VP/MeOH solutions while stirring. P2VP/OAPS/MeOH solutions were stirred for at least 24 hours before deposition and annealing, as further described below.

Differential Scanning Calorimetry (DSC): The polymer glass transition temperature (T_g) was measured via DSC with a TA Instruments Q2000. All measurements were made upon cooling a sample of ~5 mg at a rate of 10°C/min between 175°C and 25°C. T_g was defined as the inflection point of the heat flow thermograms. DSC samples were fabricated by drop casting P2VP/OAPS/MeOH solutions onto Teflon, air dried, then annealed at T=170°C under vacuum for ~24 hours. Results for T_g of P2VP/OAPS PNCs as a function of OAPS concentration and molecular weight are provided in Figure S2. T_g for bulk 100 kg/mol P2VP is measured to be ~96°C.

Broadband Dielectric Spectroscopy (BDS): Polymer reorientational segmental dynamics were measured using a Solartron ModuLab XM MTS with the femto-ammeter accessory. BDS samples were processed as described for DSC samples, but after annealing, were melt pressed to the appropriate size and placed between steel electrodes and separated with 50 µm silica spacers. Samples were annealed in the

cryostat at 160°C until the imaginary permittivity spectra at all frequencies remained constant (within 5%) over several hours. Isothermal frequency sweeps from $10^{-1} - 10^6$ Hz were measured every 3 K on cooling from 179°C to 107°C. Select measurements were made after heating again to ensure reproducibility.

Elastic Recoil Detection (ERD): The polymer chain translational diffusion coefficient was measured into P2VP/OAPS PNCs using ERD, an ion scattering technique used to measure the depth profile of light elements such as deuterium and hydrogen. Solutions containing P2VP/OAPS/MeOH were doctor bladed on a silicon wafer, air-dried, then annealed for at least 48 hours at T=160°C under vacuum. The resulting thickness was at least 20 μm. Tracer films were made by spin coating a thin layer of 2000 kg/mol polystyrene (PS) (~30 nm) on an ozone-treated silicon wafer, then a ~50 nm film of 100 kg/mol dP2VP from MeOH on the PS layer. To form the diffusion couples (Figure 1a), bilayer tracer films were floated off the silicon wafer and transferred to the pre-annealed PNC matrix for subsequent annealing at T=140°C under vacuum. Polymer diffusion couples were then measured via ERD where a He²⁺ ion beam is accelerated to 3 MeV and incident on the sample in forward scattering geometry (70° off normal), as described in detail in Ref 34 and further discussed elsewhere. 15,17 A mylar film before the detector is used to obstruct He ions but allow forward-recoiled deuterium ions to be detected.

Rutherford Backscattering Spectrometry (RBS): Nanoparticle diffusion into bulk P2VP was measured as a function of P2VP molecular weight (M_w) using RBS, an ion scattering technique used to measure the depth profile of heavy elements, such as Si herein. The P2VP matrix of varying molecular weights was doctor bladed from solutions of P2VP/MeOH on a silicon wafer and annealed for at least 48 hours at T=160°C under vacuum. The resulting thickness was at least 20 μm. The tracer films were made by spin coating a thin layer of 2000 kg/mol polystyrene (PS) (~30 nm) on an ozone-cleaned silicon wafer, followed by a ~150 nm film spin coated from the P2VP/OAPS/MeOH. Tracer films were then floated in DI water and transferred to the pre-annealed bulk P2VP matrix for subsequent annealing at T=140°C under vacuum (Figure 3a). The same P2VP M_w was used in tracer and matrix films. The OAPS concentration in the tracer film was fixed to 25 vol%. This concentration is large enough to provide sufficient Si signal in

RBS, but low enough to minimally affect polymer viscosity, and below the reported aggregation concentration.¹² OAPS diffusion couples were measured with RBS where He⁺ ions are accelerated to 3 MeV and incident normal to the sample surface. Backscattered He ions are collected at a detector 10° off normal. RBS is described in detail in Ref 34 and discussed elsewhere^{32,35}.

Results:

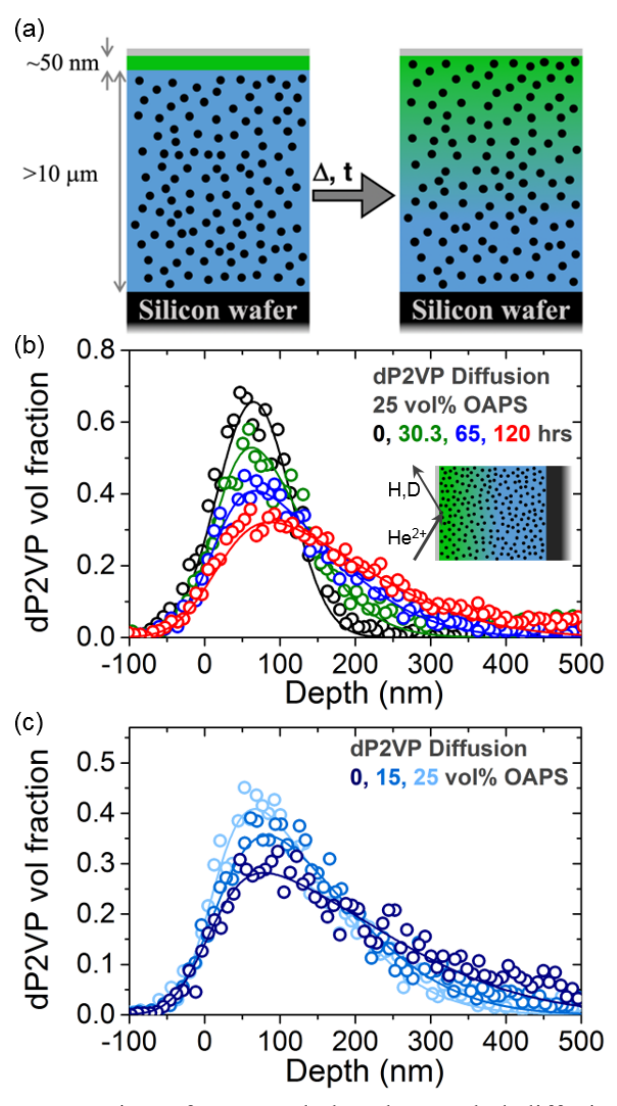


Figure 1: (a) Schematic representation of unannealed and annealed diffusion couples used to measure dP2VP diffusion into P2VP/OAPS. Measured concentration profiles from ERD of 100 kg/mol dP2VP diffused at 140°C into (b) 25 vol% OAPS PNCs after 0, 30.3, 65, and 120 hours and (c) PNCs of different NP concentrations after 65 hours. Symbols represent experimental data and solid lines represent fits used to extract diffusion coefficient. Inset of (b) depicts schematic of ERD measurement. In schematics, grey represents the sacrificial PS layer, green and blue represent dP2VP and hP2VP (respectively) and black circles represent OAPS NPs. Schematics not drawn to scale.

Polymer Dynamics. We first probe the dynamics of P2VP in P2VP/OAPS PNCs by measuring the diffusion coefficient of the chain (D_{poly}) as a function of OAPS concentration. As described elsewhere ^{15,17} and schematically depicted in Figure 1a, elastic recoil detection (ERD) was used to measure the depth profile of 100 kg/mol dP2VP ($M/M_e\sim5.5$, $R_g\sim8.6$ nm) as it diffuses into PNC films with different NP concentrations after different annealing times. At OAPS concentrations of 25 vol%, the highest concentrations studied here, yet still below the previously reported aggregation threshold ¹², the expected NP-NP separation distance for randomly packed OAPS ($R_{NP}=0.9$ nm) is only ~2.5 nm. We confirm reasonable OAPS dispersion in P2VP using X-ray scattering between 2 Å and 370 nm, as described in Figure S3. Furthermore, measured Si depth profiles in Figure S4 show uniform distribution of OAPS through the depth of the film with no measurable surface aggregation. OAPS dispersion at NP concentrations up to 25 vol%, which is not common in PNCs containing POSS^{36,37}, suggests strong and favorable NP-polymer interactions between OAPS and P2VP. ^{12,33}

Representative diffusion profiles of dP2VP diffusing into P2VP with 25 vol% OAPS at 140°C at various diffusion times are shown in Figure 1b. As expected, dP2VP diffuses farther into the underlying matrix after longer annealing times. The dP2VP diffusion coefficient is extracted from the experimental data by fitting each concentration profile with Fick's second law describing a finite source diffusing into a semi-infinite medium. Figure 1c displays dP2VP profiles measured at the same annealing temperature and time as a function of OAPS concentration. For the same annealing conditions, dP2VP diffusion is slowed as the NP concentration in the underlying matrix is increased. The extracted polymer diffusion coefficients as a function of NP concentration are shown in Figure 2a. The error bars, which are smaller than the size of the data points, are calculated from the standard deviation of at least three annealing times.

Whereas the addition of small molecules³⁹, including POSS³⁷, often enhances dynamics and plasticizes a polymer melt, we observe the opposite effect in this attractive mixture. The observed monotonic reduction in D_{poly} can be qualitatively understood by a slowing of segmental dynamics and increase in glass transition temperature, as previously reported in the same system.¹² To compare dynamics at the segment and chain-scale, the segmental reorientational relaxation time (τ_{α}) was measured by

dielectric spectroscopy at 140°C and is presented in Figure 2a (see Figure S5 for dielectric measurements at various temperatures). As the OAPS concentration increases, τ_{α} increases showing slower relaxations, consistent with DSC measurements (Figure S2) and literature.¹²

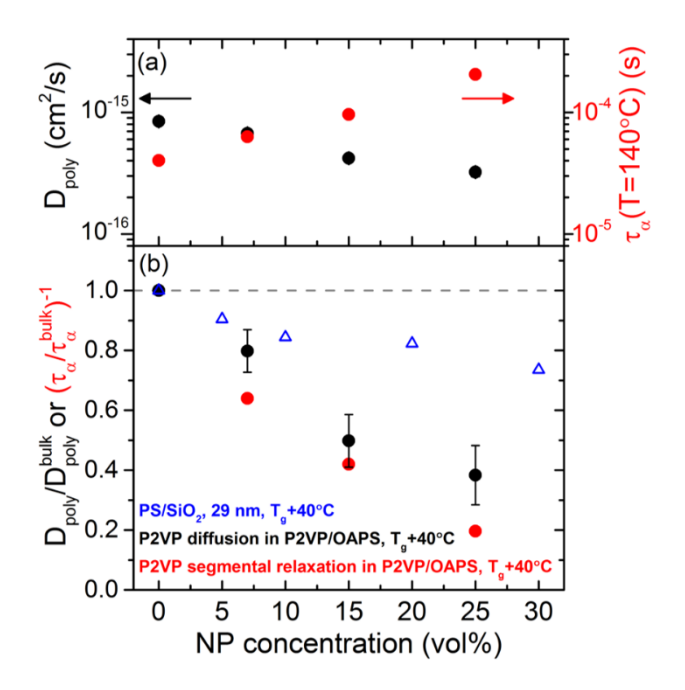


Figure 2: Measured dP2VP diffusion coefficient (black) and segmental relaxation times (red) as a function of OAPS concentration ($M_w = 100 \text{ kg/mol}$ and $T = 140^{\circ}\text{C}$). (b) Normalized P2VP diffusion coefficient (black) and segmental relaxation time (red) as a function of NP concentration. Included for comparison in (b) is polystyrene diffusion in PNCs with immobile, athermal NPs ($R_{NP} = 15 \text{ nm}$) at $T = 140^{\circ}\text{C}$ (blue).⁴⁰

By comparing the normalized chain and segmental dynamics in PNCs to bulk P2VP in Figure 2b, we find the addition of these Kuhn bead-sized NPs slows segmental dynamics slightly more than chain dynamics. For example, at the highest NP loading, chain diffusion is slowed by ~60% relative to bulk, while the segmental dynamics are slowed by ~80%. To further understand these reductions in polymer dynamics, we interpret our results in terms of the reptation model, where polymer diffusion in an entangled matrix is defined as:

$$D_{poly} \approx \frac{R_{ee}^2}{\tau_{ren}} \approx \frac{R_{ee}^2}{N^2} \left(\frac{k_B T}{\xi b^2}\right) \frac{N_e}{N} \propto \frac{R_{ee}^2 N_e}{N^3 \tau_{cc}} \frac{1}{\tau_{cc}}$$
(2)

where R_{ee} is the polymer end-to-end distance, N is the degree of polymerization, N_e is the degree of polymerization of an entanglement strand, ξ is the monomeric friction coefficient, and b is the Kuhn length.²⁵ The term $k_BT/\xi b^2$ is proportional to the segmental relaxation rate, τ_{α}^{-1} (Equation 2).²⁵ Thus,

according to the reptation model, the observed differences between D_{poly} and τ_{α} in Figure 2b could be related to dilation of chain dimensions (increasing R_{ee}) or disentanglement effects (increasing N_e). Recent small angle neutron scattering experiments on a similar system of poly(methyl methacrylate) and weakly attractive POSS observed no change in R_{ee} in PNCs relative to bulk.³⁶ Thus, it is unlikely that differences in chain dimensions are responsible for differences in polymer dynamics in our system. Moreover, disentanglement has been observed in recent rheology measurements of this P2VP/OAPS system.¹² Furthermore, in an athermal system of poly(ethylene oxide) and small gold NPs, neutron scattering also revealed tube dilation of ~20% at a NP concentration of 20 vol%.⁴¹ Given these observations, we surmise that the observed enhancements in D_{poly} relative to τ_{α} are primarily related to disentanglement and tube dilation likely resulting from excluded volume, but the specific impact of NP-polymer attraction in our system remains unclear. Figure 2b also includes a quantitative comparison to the reduction in chain-scale diffusion of polystyrene (PS) diffusing into athermal PNCs comprised of PS and phenyl-capped SiO₂ (SiO₂-Ph, $R_{NP} = 15$ nm).⁴⁰ At T = 140°C and at all ϕ_{NP} , the addition of small OAPS into P2VP (attractive) is more impactful and more dependent on ϕ_{NP} than the addition of larger SiO₂-Ph into PS (athermal).⁴⁰

Nanoparticle Dynamics. To fully understand the dynamics in these attractive P2VP/OAPS PNCs, we next measure the diffusion of OAPS NPs in P2VP of various molecular weights. As described elsewhere^{32,35} and shown schematically in Figure 3a, Rutherford backscattering spectrometry (RBS) was used to measure the depth profile of OAPS infiltration into bulk P2VP. A representative set of fitted diffusion profiles for OAPS diffusion into 90 kg/mol P2VP at 140°C is presented in Figure 3b. OAPS diffusion was measured in seven P2VP melts (2R_{NP}/d_{tube}~0.25) with M_w ranging from 28 to 467 kg/mol spanning M/M_e~1 to 26 and R_g/R_{NP}~5 to 21, as listed in Table S1.

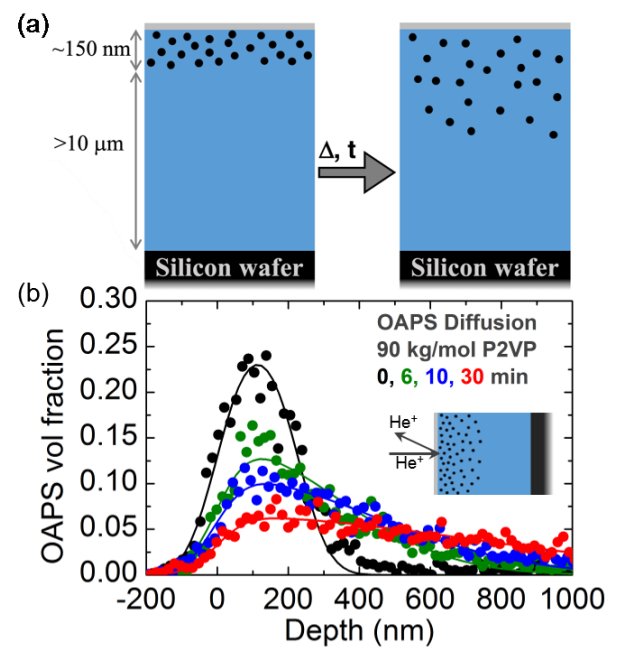


Figure 3: (a) Schematic of unannealed and annealed diffusion couples used to measure OAPS diffusion into bulk P2VP polymer melts. (b) Representative concentration profiles from RBS of OAPS in 90 kg/mol P2VP after 0, 6, 10, and 30 minutes at 140°C. Inset of (b) depicts schematic of RBS. In schematics, grey represents the sacrificial PS layer, blue represents P2VP and black circles represent OAPS NPs. Schematics not drawn to scale.

The measured D_{OAPS} presented in Figure 4a monotonically decreases with increasing P2VP M_w , but only weakly, scaling as $M_w^{-0.7\pm0.1}$. Furthermore, these NP diffusion coefficients are substantially larger than those predicted by SE (D_{SE} , Equation 1), calculated using the zero-shear viscosity (η_0) of bulk P2VP³² (see Figure S6 for details). Recent rheology measurements¹² of P2VP/OAPS showed only a subtle change in η_0 upon the addition of up to 25 vol% OAPS, which is equivalent to the maximum local OAPS concentration in unannealed tracer films and more concentrated than the local environment OAPS NPs experience during these diffusion measurements (~5 vol%, Figure 3b). We have verified the negligible change in η_0 (~30% increase relative to bulk) in 5 vol% OAPS PNCs using small amplitude oscillatory shear measurements (Figure S6).

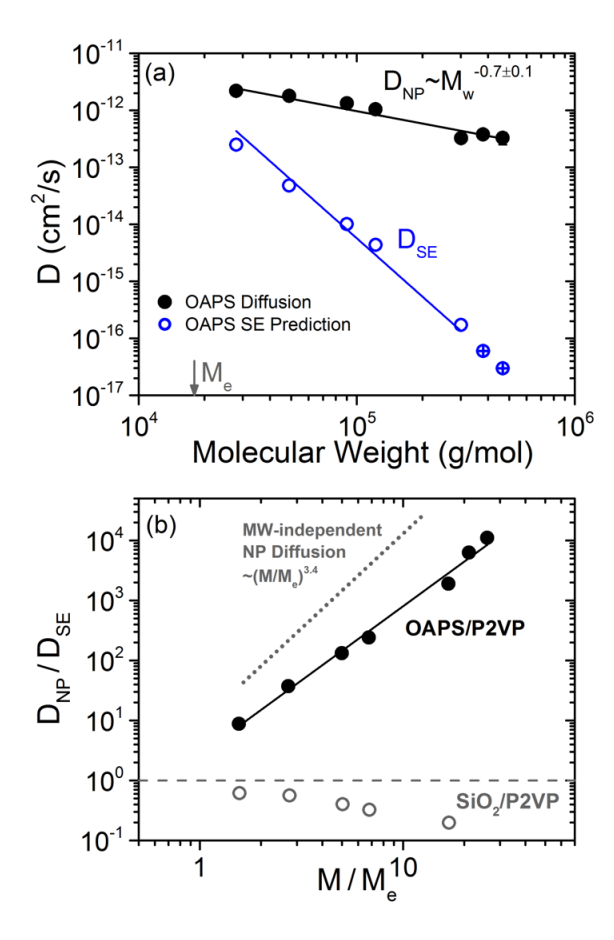


Figure 4: (a) Measured OAPS NP diffusion coefficient (solid black circles) and Stokes-Einstein prediction (blue open circles) as a function of P2VP molecular weight. Data shown in blue circles with crosses were calculated using extrapolated values of η_0 , as described in Figure S6. (b) OAPS diffusion coefficient normalized to SE prediction as a function of number of entanglements per chain (solid black circles). Earlier experimental measurements³² (open circles) of larger attractive NPs ($R_{NP} = 13$ nm) are shown for comparison.

In this attractive P2VP/OAPS system, we observe fast NP diffusion relative to SE (D_{OAPS}/D_{SE}) by 10^1 – 10^4 over the molecular weight range studied (Figure 4b). These results are consistent with an extrapolation to large M_w of the recent DLS study of a similar system (OAPS in PPG) that found a crossover from $D < D_{SE}$ to $D > D_{SE}$ at $R_g \sim R_{NP}$ (as well as $M \sim M_e$).³³ In stark contrast to our previous studies of SiO₂ NP diffusion ($R_{NP} = 13$ nm) in P2VP that diffuse via the core-shell mechanism (Figure 4b, open circles), decreasing the size of the NP by a factor of ~14 changes D/D_{SE} by up to 10^4 at high M_w (Figure 4b).³² This clearly demonstrates the fundamental importance of NP size on transport mechanisms.

The weak molecular weight dependence found for D_{OAPS} in P2VP/OAPS PNCs suggests that NP motion is coupled to polymer dynamics between segmental relaxations (approximately M_w independent) and longer-range Rouse relaxations (scaling with M_w^{-1}) and is decoupled from chain-scale relaxations (scaling with $M_w^{-3.4}$). Recent theoretical predictions by Yamamoto et al. predict that small NPs with enthalpic attraction to the polymer matrix diffuse in entangled polymers via a vehicular mechanism. ²⁶ In vehicle diffusion, NPs diffuse with the local polymer environment until successive desorption and adsorption events lead to Fickian NP diffusion. ²⁶ The frequency of desorption events and lifetime of NP-polymer adsorption depend on system-specific parameters, especially NP size and NP-polymer interaction. Although the NP-polymer interaction and desorption time in P2VP/OAPS are difficult to experimentally probe, our observations that NP motion is coupled to subdiffusive polymer relaxations (Figure 4a) support the theory of vehicle diffusion.

Discussion:

By directly measuring the dynamics of polymer segments, the chain, and the NPs in this P2VP/OAPS model system, we can quantitatively and mechanistically understand how small, enthalpically-attractive NPs diffuse in entangled polymer melts and how they impact polymer dynamics at various length scales. Figure 5 summarizes and quantitatively compares directly measured or estimated polymer and nanoparticle dynamics in this P2VP/OAPS system.

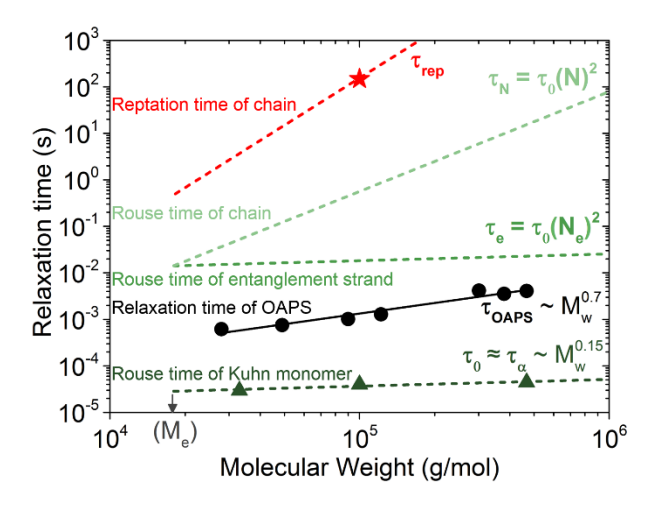


Figure 5: Comparison of relaxation times for P2VP at various length scales and OAPS NPs as a function of M_w . The Rouse times of a Kuhn monomer are taken directly from BDS measurements of bulk P2VP and are used to calculate the Rouse time of an entanglement strand and the chain. The P2VP reptation time and OAPS relaxation time are calculated directly from ERD and RBS measurements, respectively. All measurements are made at 140° C.

We consider the segmental relaxation time (τ_{α}) to be approximately equal to the relaxation time of a single Kuhn monomer, and therefore the shortest Rouse time of P2VP (τ_0) . According to the Rouse model²⁵, the relaxation time of an entanglement strand (τ_e) is given by $\tau_e = \tau_0(N_e)^2$ where N_e for P2VP^{12,32,42} is ~23. Our assignment of τ_0 is supported by recent rheology and dielectric measurements of bulk P2VP, which found $\tau_e/\tau_\alpha \sim 10^3$ or $\sim N_e^2$.¹² Although τ_α is often considered molecular weight independent, we measure a weak M_w dependence of τ_α in bulk P2VP at 140°C, scaling with $M_w^{0.15}$, which follows the slight increase in T_g (Figures S2 and S7). The reptation time of the chain (τ_{rep}) can be calculated from the measured diffusion coefficient in Figure 2a through $\tau_{rep} = (R_g)^2/(6\cdot D_{poly})$, and is expectedly slower than the Rouse prediction (τ_N) which neglects entanglement effects. Similarly, the relaxation time of the OAPS NPs can

be calculated as $\tau_{OAPS} = (R_{NP})^2/(6 \cdot D_{OAPS})$. The measured τ_0 and τ_{rep} data shown in Figure 5 are for 100 kg/mol bulk P2VP (Figure 2a) and all measurements presented are at 140°C.

With experimental evidence that OAPS diffusion is slower than Kuhn segment relaxations but faster than P2VP chain diffusion, we can further understand the polymer dynamic results presented in Figure 2. For traditional PNCs (such as PS/SiO₂-Ph), the slowing of chain diffusion has been described with excluded volume⁴³ and entropic^{15,40} arguments. However, chain-scale entropic effects can be considered negligible in P2VP/OAPS diffusion, because the OAPS position is fully decorrelated on the timescale of conformation fluctuations ($\sim \tau_{rep}$), NPs fully penetrate polymer conformations, and all chains likely sample similar conformations. These justifications are not true for larger and less mobile NPs. Furthermore, in PNCs with larger NPs ($R_{NP} \ge R_g$), the mean molecular relaxation time is largely unchanged overall^{44,45}, even though friction is known to be significantly increased at the NP-polymer interface¹³. As a result, while segmental relaxations are less perturbed than chain diffusion in traditional PNCs, the perturbations are similar in P2VP/OAPS PNCs (Figure 2b), thus highlighting the fundamentally different mechanism causing reduced chain-scale polymer diffusion in PNCs with small, attractive, and highly mobile NPs.

In P2VP/OAPS PNCs, we conclude that polymer segments and small NPs relax together making the segments slower than in bulk and significantly increasing the friction on the chain. This conclusion is supported by observations that the step in heat capacity at T_g remains unchanged upon the addition of OAPS NPs¹², which we confirm in our DSC measurements, suggesting that these small and attractive NPs are dynamically active during segmental relaxations. Since the friction at the segmental scale is increased, chain-scale diffusion is similarly slowed while also being slightly enhanced by other factors (e.g. disentanglement, Equation 2). This mechanism of chain-scale retardation through segmental friction is categorically different than previous measurements of polymer diffusion in PNCs with larger SiO₂ ($R_{NP} > 6$ nm) and likely results from the enthalpic attraction, size, and mobility of OAPS NPs. $R_{NP} > 15-18,40$

Given that these attractive OAPS NPs are coupled to M_w -dependent polymer dynamics (Figure 4a), and the measured OAPS diffusion is faster than the P2VP chain diffusion (Figure 5), we conclude that NP desorption from the P2VP chain occurs. Since $\tau_0 < \tau_{OAPS} < \tau_e$ for all M_w P2VP (Figure 5), the desorption time of OAPS NPs (τ_{des}) must also lie somewhere between the Rouse time of a single Kuhn bead and that of an entanglement strand. For systems with this dynamic behavior (specifically $\tau_{\alpha} < \tau_{des} < \tau_{rep}$) recent theory predicts vehicle diffusion and D_{NP} scaling of $M_w^{-0.5}$. Figure 4a, for OAPS diffusion in P2VP, shows qualitative and also approximate quantitative agreement with this theory (scaling with $M_w^{-0.7\pm0.1}$). Importantly, the prediction of $D_{NP} \sim M_w^{-0.5}$ assumes M_w -independent segmental relaxations²⁶, thus, the slightly larger exponent observed experimentally can be attributed to the M_w -dependence of segmental dynamics ($D_{\alpha} \sim M_w^{-0.15}$, Figure S7). Further potential differences in theoretical predictions and experimental measurements are expected from differences in the NP-polymer interaction strength and the exact timescales of τ_{des} and τ_0 .

Although our dynamic measurements provide support of vehicular diffusion, to fully and definitively prove this mechanism, additional measurements must be conducted by altering the NP desorption time, potentially through changes in NP size, NP surface chemistry, or temperature (in the case of hydrogen bonding PNC systems). As NP desorption is slowed through increasing R_{NP} or strengthening the NP-polymer interaction, a stronger molecular weight dependence and smaller D/D_{SE} can be expected as the NPs will be more coupled to polymer dynamics.^{26,32} Independently controlling NP-polymer interaction strength (without significantly changing NP dispersion) and NP size (without significantly changing the NP-polymer interactions) remains an experimental challenge.^{1–3}

Conclusion

Polymer segmental dynamics, polymer chain dynamics, and NP diffusion coefficients, were directly measured in mixtures of entangled P2VP (M/Me \sim 1 – 26) and OAPS (R_{NP} = 0.9 nm), which exhibit favorable NP-polymer interactions. In this system, the P2VP chain diffusion slows by \sim 60% relative to bulk at 25 vol% OAPS, an effect consistent with increased friction at the segmental scale with potential contributions from disentanglement. In addition, OAPS NPs diffuse at timescales between polymer segmental dynamics and chain-scale diffusion and D_{OAPS} is weakly dependent on molecular weight, scaling with $M_w^{-0.7\pm0.1}$. We observe enhancements in D_{OAPS} relative to hydrodynamic Stokes-Einstein predictions of up to 10^4 , providing experimental support of recent theoretical predictions describing vehicle diffusion in well-entangled polymer melts. ²⁶ By measuring polymer and NP dynamics, we show that small attractive NPs diffuse with polymer segments commensurate with the NP size, thereby slowing the polymer segmental motion and other dynamic processes (e.g. reptation) that occur at longer length and time scales. We conclude that in this attractive PNC system with small NPs and entangled polymers, successive adsorption/desorption events on Rouse-like timescales lead to NP diffusion coupled to sub-diffusive polymer dynamics but decoupled from the polymer chain diffusion, as proposed by the vehicular mechanism.

Associated Content

Supporting Information:

Description of materials, glass transition measurements of P2VP/OAPS as a function of NP

concentration and molecular weight, X-ray scattering measurements of P2VP/OAPS, OAPS depth

concentration in annealed matrix PNCs, dielectric spectra of PNCs at 140°C and extracted segmental

relaxation times at other temperatures, rheology of P2VP/OAPS, and dielectric measurements at 140°C of

bulk P2VP at various molecular weights (PDF)

Author Information

Corresponding Author:

* Email: winey@seas.upenn.edu (K.I.W.).

Author Contributions:

‡ E. J. Bailey and P. J. Griffin contributed equally to this work.

Present Addresses:

PJG: Institute for Molecular Engineering, University of Chicago, Chicago, IL 60637.

ORCID:

Eric J. Bailey: 0000-0001-7194-9035

Russell J. Composto: 0000-0002-5906-2594

Karen I. Winey: 0000-0001-5856-3410

Notes:

The authors declare no competing financial interest.

Acknowledgments

EJB and KIW acknowledge support from NSF-CBET #1706014. EJB acknowledges primary

support from the National Science Foundation Graduate Research Fellowship Program under Grant No.

DGE-1321851. Any opinions, findings, and conclusions or recommendations expressed in this material are

those of the authors and do not necessarily reflect the views of the National Science Foundation. ERD and

RBS measurements were performed at the University of Pennsylvania's Nanoscale Characterization

20

Facility, an NNCI member supported by NSF Grant ECCS-1542153, and we thank Doug Yates for assistance with these measurements. The authors acknowledge use of the Dual Source and Environmental X-ray Scattering facility operated by the Laboratory for Research on the Structure of Matter at the University of Pennsylvania (NSF MRSEC 17-20530). The equipment purchase was made possible by a NSF MRI grant (17-25969), a ARO DURIP grant (W911NF-17-1-0282), and the University of Pennsylvania. The authors are grateful to Dr. Vera Bocharova (Oak Ridge National Laboratory) for generously providing dry OAPS powder. The authors would like to thank Leshang Wang and Peter Gordon for GPC measurements of 100 kg/mol P2VP and dP2VP, Nicholas Han for assistance with preliminary dielectric measurements and analysis, and Lu Yan and Steve Szewczyk for additional assistance.

References

- (1) Kumar, S. K.; Benicewicz, B. C.; Vaia, R. A.; Winey, K. I. 50th Anniversary Perspective: Are Polymer Nanocomposites Practical for Applications? *Macromolecules* **2017**, *50*, 714–731.
- (2) Kumar, S. K.; Ganesan, V.; Riggleman, R. A. Perspective: Outstanding Theoretical Questions in Polymer-Nanoparticle Hybrids. *J. Chem. Phys.* **2017**, *147* (2).
- (3) Cheng, S.; Carroll, B.; Bocharova, V.; Carrillo, J.-M.; Sumpter, B. G.; Sokolov, A. P. Focus: Structure and Dynamics of the Interfacial Layer in Polymer Nanocomposites with Attractive Interactions. *J. Chem. Phys.* **2017**, *146* (20), 203201.
- (4) Lin, C. C.; Parrish, E.; Composto, R. J. Macromolecule and Particle Dynamics in Confined Media. *Macromolecules* **2016**, *49* (16), 5755–5772.
- (5) LaVan, D. A.; McGuire, T.; Langer, R. Small-Scale Systems for in Vivo Drug Delivery. *Nat. Biotechnol.* **2003**, *21* (10), 1184–1191.
- (6) Robertson, C. G.; Roland, C. M. Glass Transition and Interfacial Segmental Dynamics in Polymer-Particle Composites. *Rubber Chem. Technol.* **2008**, *81* (3), 506–522.
- (7) Priestley, R. D.; Cangialosi, D.; Napolitano, S. On the Equivalence between the Thermodynamic and Dynamic Measurements of the Glass Transition in Confined Polymers. *J. Non. Cryst. Solids* **2015**, *407*, 288–295.
- (8) Bailey, E. J.; Griffin, P. J.; Tyagi, M.; Winey, K. I. Segmental Diffusion in Attractive Polymer Nanocomposites: A Quasi-Elastic Neutron Scattering Study. *Macromolecules* **2019**, *52* (2), 669–678.
- (9) Holt, A. P.; Bocharova, V.; Cheng, S.; Kisliuk, A. M.; White, B. T.; Saito, T.; Uhrig, D.; Mahalik, J. P.; Kumar, R.; Imel, A. E.; et al. Controlling Interfacial Dynamics: Covalent Bonding versus Physical Adsorption in Polymer Nanocomposites. *ACS Nano* **2016**, *10* (7), 6843–6852.
- (10) Holt, A. P.; Sangoro, J. R.; Wang, Y.; Agapov, A. L.; Sokolov, A. P. Chain and Segmental Dynamics of Poly(2-Vinylpyridine) Nanocomposites. *Macromolecules* **2013**, *46* (10), 4168–4173.
- (11) Gong, S.; Chen, Q.; Moll, J. F.; Kumar, S. K.; Colby, R. H. Segmental Dynamics of Polymer Melts with Spherical Nanoparticles. *ACS Macro Lett.* **2014**, *3* (8), 773–777.
- (12) Cheng, S.; Xie, S.-J.; Carrillo, J.-M. Y.; Carroll, B.; Martin, H.; Cao, P.-F.; Dadmun, M. D.; Sumpter, B. G.; Novikov, V. N.; Schweizer, K. S.; et al. Big Effect of Small Nanoparticles: A Shift in Paradigm for Polymer Nanocomposites. *ACS Nano* **2017**, *11*, 752–759.
- (13) Holt, A. P.; Griffin, P. J.; Bocharova, V.; Agapov, A. L.; Imel, A. E.; Dadmun, M. D.; Sangoro, J. R.; Sokolov, A. P. Dynamics at the Polymer/Nanoparticle Interface in Poly(2-Vinylpyridine)/Silica Nanocomposites. *Macromolecules* **2014**, *47* (5), 1837–1843.
- (14) Starr, F. W.; Douglas, J. F.; Meng, D.; Kumar, S. K. Bound Layers "Cloak" Nanoparticles in Strongly Interacting Polymer Nanocomposites. *ACS Nano* **2016**, *10* (12), 10960–10965.
- (15) Gam, S.; Meth, J. S.; Zane, S. G.; Chi, C.; Wood, B. a.; Seitz, M. E.; Winey, K. I.; Clarke, N.; Composto, R. J. Macromolecular Diffusion in a Crowded Polymer Nanocomposite. *Macromolecules* **2011**, *44* (9), 3494–3501.
- (16) Gam, S.; Meth, J. S.; Zane, S. G.; Chi, C.; Wood, B. A.; Winey, K. I.; Clarke, N.; Composto, R. J. Polymer Diffusion in a Polymer Nanocomposite: Effect of Nanoparticle Size and Polydispersity. *Soft Matter* **2012**, *8* (24), 6512–6520.
- (17) Lin, C.; Gam, S.; Meth, S.; Clarke, N.; Winey, K. I.; Composto, R. J. Do Attractive Polymer Nanoparticle Interactions Retard Polymer Diffusion in Nanocomposites? *Macromolecules* **2013**, 46, 4502–4509.
- (18) Choi, J.; Hore, M. J. a; Meth, J. S.; Clarke, N.; Winey, K. I.; Composto, R. J. Universal Scaling of Polymer Diffusion in Nanocomposites. *ACS Macro Lett.* **2013**, *2* (6), 485–490.
- (19) Lin, C.-C.; Cargnello, M.; Murray, C. B.; Clarke, N.; Winey, K. I.; Riggleman, R. A.; Composto, R. J. Nanorod Mobility Influences Polymer Diffusion in Polymer Nanocomposites. *ACS Macro Lett.* **2017**, *6*, 869–874.
- (20) Cai, L. H.; Panyukov, S.; Rubinstein, M. Hopping Diffusion of Nanoparticles in Polymer

- Matrices. Macromolecules 2015, 48 (3), 847-862.
- (21) Yamamoto, U.; Schweizer, K. S. Microscopic Theory of the Long-Time Diffusivity and Intermediate-Time Anomalous Transport of a Nanoparticle in Polymer Melts. *Macromolecules* **2015**, *48* (1), 152–163.
- (22) Dell, Z. E.; Schweizer, K. S. Theory of Localization and Activated Hopping of Nanoparticles in Cross-Linked Networks and Entangled Polymer Melts. *Macromolecules* **2014**, *47* (1), 405–414.
- (23) Mangal, R.; Srivastava, S.; Narayanan, S.; Archer, L. A. Size-Dependent Particle Dynamics in Entangled Polymer Nanocomposites. *Langmuir* **2016**, *32* (2), 596–603.
- Tuteja, A.; Mackay, M. E.; Narayanan, S.; Asokan, S.; Wong, M. S. Breakdown of the Continuum Stokes-Einstein Relation for Nanoparticle Diffusion. *Nano Lett.* **2007**, *7* (5), 1276–1281.
- (25) Rubinstein, M.; Colby, R. H. Polymer Physics; Oxford University Press: Oxford, 2003.
- (26) Yamamoto, U.; Carrillo, J. M. Y.; Bocharova, V.; Sokolov, A. P.; Sumpter, B. G.; Schweizer, K. S. Theory and Simulation of Attractive Nanoparticle Transport in Polymer Melts. *Macromolecules* **2018**, *51* (6), 2258–2267.
- (27) Brochard Wyart, F.; de Gennes, P. G. Viscosity at Small Scales in Polymer Melts. *Eur. Phys. J. E Soft Matter* **2000**, *I* (1), 93–97.
- (28) Crawford, M. K.; Smalley, R. J.; Cohen, G.; Hogan, B.; Wood, B.; Kumar, S. K.; Melnichenko, Y. B.; He, L.; Guise, W.; Hammouda, B. Chain Conformation in Polymer Nanocomposites with Uniformly Dispersed Nanoparticles. *Phys. Rev. Lett.* **2013**, *110* (19), 1–5.
- (29) Grabowski, C. A.; Mukhopadhyay, A. Size Effect of Nanoparticle Diffusion in a Polymer Melt. *Macromolecules* **2014**, *47* (20), 7238–7242.
- (30) Kalathi, J. T.; Yamamoto, U.; Schweizer, K. S.; Grest, G. S.; Kumar, S. K. Nanoparticle Diffusion in Polymer Nanocomposites. *Phys. Rev. Lett.* **2014**, *112* (10), 1–5.
- (31) Liu, J.; Cao, D.; Zhang, L. Molecular Dynamics Study on Nanoparticle Diffusion in Polymer Melts: A Test of the Stokes-Einstein Law. *J. Phys. Chem. C* **2008**, *112* (17), 6653–6661.
- (32) Griffin, P. J.; Bocharova, V.; Middleton, L. R.; Composto, R. J.; Clarke, N.; Schweizer, K. S.; Winey, K. I. Influence of the Bound Polymer Layer on Nanoparticle Diffusion in Polymer Melts. *ACS Macro Lett.* **2016**, *5* (10), 1141–1145.
- (33) Carroll, B.; Bocharova, V.; Carrillo, J. M. Y.; Kisliuk, A.; Cheng, S.; Yamamoto, U.; Schweizer, K. S.; Sumpter, B. G.; Sokolov, A. P. Diffusion of Sticky Nanoparticles in a Polymer Melt: Crossover from Suppressed to Enhanced Transport. *Macromolecules* **2018**, *51* (6), 2268–2275.
- (34) Composto, R. J.; Walters, R. M.; Genzer, J. Application of Ion Scattering Techniques to Characterize Polymer Surfaces and Interfaces. *Mater. Sci. Eng. R Reports* **2002**, *38* (3–4), 107–180.
- (35) Lin, C. C.; Griffin, P. J.; Chao, H.; Hore, M. J. A.; Ohno, K.; Clarke, N.; Riggleman, R. A.; Winey, K. I.; Composto, R. J. Grafted Polymer Chains Suppress Nanoparticle Diffusion in Athermal Polymer Melts. *J. Chem. Phys.* **2017**, *146* (20).
- (36) Jouault, N.; Kumar, S. K.; Smalley, R. J.; Chi, C.; Moneta, R.; Wood, B.; Salerno, H.; Melnichenko, Y. B.; He, L.; Guise, W. E.; et al. Do Very Small POSS Nanoparticles Perturb S-PMMA Chain Conformations? *Macromolecules* **2018**, *51*, acs.macromol.8b00432.
- (37) Ayandele, E.; Sarkar, B.; Alexandridis, P. Polyhedral Oligomeric Silsesquioxane (POSS)-Containing Polymer Nanocomposites. *Nanomaterials* **2012**, *2* (4), 445–475.
- (38) Crank, J. The Mathematics of Diffusion; Oxford University Press: New York, 1975.
- (39) Nambiar, R. R.; Blum, F. D. Segmental Dynamics of Bulk Poly(Vinyl Acetate)-D3 by Solid-State 2H NMR: Effect of Small Molecule Plasticizer. **2008**, *41*, 9837–9845.
- (40) Tung, W.-S.; Griffin, P. J.; Meth, J. S.; Clarke, N.; Composto, R. J.; Winey, K. I. Temperature-Dependent Suppression of Polymer Diffusion in Polymer Nanocomposites. *ACS Macro Lett.* **2016**, 735–739.
- (41) Senses, E. Small Particle Driven Chain Disentanglements in Polymer Nanocomposites. *Phys. Rev. Lett.* **2017**, *118* (14), 147801.
- (42) Cheng, S.; Carroll, B.; Lu, W.; Fan, F.; Carrillo, J. M. Y.; Martin, H.; Holt, A. P.; Kang, N. G.;

- Bocharova, V.; Mays, J. W.; et al. Interfacial Properties of Polymer Nanocomposites: Role of Chain Rigidity and Dynamic Heterogeneity Length Scale. *Macromolecules* **2017**, *50* (6), 2397–2406
- (43) Meth, J. S.; Gam, S.; Choi, J.; Lin, C. C.; Composto, R. J.; Winey, K. I. Excluded Volume Model for the Reduction of Polymer Diffusion into Nanocomposites. *J. Phys. Chem. B* **2013**, *117* (49), 15675–15683.
- (44) Holt, A. P.; Sangoro, J. R.; Wang, Y.; Agapov, A. L.; Sokolov, A. P. Chain and Segmental Dynamics of Poly (2-Vinylpyridine) Nanocomposites. *Macromolecules* **2013**, *46*, 4168.
- (45) Meth, J. S.; Zane, S. G.; Chi, C.; Londono, J. D.; Wood, B. A.; Cotts, P.; Keating, M.; Guise, W.; Weigand, S. Development of Filler Structure in Colloidal Silica-Polymer Nanocomposites. *Macromolecules* **2011**, *44* (20), 8301–8313.